Hindawi
Adsorption Science & Technology
Volume 2021, Article ID 5527594, 11 pages
https://doi.org/10.1155/2021/5527594

Research Article

Adsorptive Performance of Polypyrrole-Based KOH-Activated Carbon for the Cationic Dye Crystal Violet: Kinetic and Equilibrium Studies

Abdulaziz Ali Alghamdi,[1] **Abdel-Basit Al-Odayni**,[2] **Naaser A. Y. Abduh**,[1] **Safiah A. Alramadhan**,[1] **Mashael T. Aljboar**,[1] **and Waseem Sharaf Saeed**[2]

[1]*Department of Chemistry, College of Science, King Saud University, P.O. Box 2455, Riyadh 11451, Saudi Arabia*
[2]*Engineer Abdullah Bugshan Research Chair for Dental and Oral Rehabilitation, College of Dentistry, King Saud University, Riyadh 11545, Saudi Arabia*

Correspondence should be addressed to Abdel-Basit Al-Odayni; aalodayni@ksu.edu.sa

Received 14 May 2020; Accepted 25 February 2021; Published 20 March 2021

Academic Editor: Danina Krajišnik

The aim of this work was to investigate the adsorptive performance of the polypyrrole-based KOH-activated carbon (PACK) in the removal of the basic dye crystal violet (CV) using a batch adsorption system. The equilibrium data, obtained at different initial CV concentrations (C_0 = 50 – 500 mg/L) and temperatures (25–45°C), were interpreted using the Langmuir, Freundlich, Temkin, and Dubinin-Radushkevich isotherms, with the Langmuir model providing a better fit ($R^2 \geq 0.9997$) and a maximum adsorption capacity of 497.51 mg/g at 45°C. Under the examined conditions, the values of the thermodynamic parameters free energy, enthalpy, and entropy indicate a spontaneous, endothermic, and physisorption adsorption process. The kinetic data of the adsorption process were very well described by a pseudo-second-order model ($R^2 \geq 0.9996$). However, surface diffusion seems to be the main rate-controlling step. Thus, we concluded that PACK shows commercial potential for the removal of cationic dyes such as CV from industrial effluent.

1. Introduction

Water pollution is a major environmental problem worldwide and requires urgent solutions. Industrial discharge is the main source of aquatic pollution [1] and results in the release of various physical, chemical, and biological pollutants, including suspended elements, dissolved gasses, mineral and organic solutes, and microorganisms [2]. The effluents from the paper, textile, leather, food, plastic, pharmaceutical, and printing industries typically contain large quantities of dyes that are used to color their products. Although many of the dyes used are not highly toxic, they cause visual pollution via aesthetic changes to the natural environment. Furthermore, they cause a reduction in light penetration into water, impinging on the photosynthesis of aquatic organisms. Nevertheless, many dyes have long-lasting hazardous and toxic effects on aquatic life, largely due to their high water solubility and nondegradability under natural conditions [3].

Crystal violet (CV), also known as gentian violet, is a synthetic cationic dye belonging to the triphenylmethane group. Compared with anionic dyes, cationic dyes are more toxic to mammalian cells due to their ability to interact with negatively charged cell membrane surfaces, which enables them to penetrate into cells and concentrate in the cytoplasm [4]. CV is used in a variety of applications, including textile, plastic, and paper coloring; biological staining; and veterinary and animal medicine. However, researchers have reported that CV is a mutagen and mitotic poison that is toxic to mammalian cells and may exhibit carcinogenic effects [5–8]. Moreover, it can cause irritation to the skin and digestive tract. In extreme cases, CV can cause kidney

failure and severe eye irritation leading to permanent blindness [9, 10]. These harmful effects necessitate efficient strategies for the removal of CV (and similar toxic dyes) from water bodies.

Numerous methods have been developed for removing dyes from contaminated wastewater, including adsorption-based strategies, membrane filtration, photodegradation, coagulation, chemical oxidation, and biological processes [6, 11–13]. Among these, adsorption is the most common technique due to its numerous advantages, which include its superior performance, ease of operation, cost effectiveness, and the availability of necessary reagents. Furthermore, it has been widely demonstrated that activated carbon is the most effective adsorbent of the various applicable materials, which include natural clays, zeolites, biomasses, polymers, and polymer-based materials [14].

Nitrogen-doped polypyrrole-based activated carbons (termed PACK), which is applied here for the removal of CV as a model harmful cationic dye, have been demonstrated to be excellent adsorbents. Various studies have indicated their high capacity in the adsorption of gasses including nitrogen and carbon dioxide, toxic heavy metal ions such as Pb(II), and anionic dyes such as methyl orange [15–18].

The objective of the present study was to evaluate the efficiency of PACK in the removal of CV from synthetic wastewater. Its adsorption kinetics, isotherms, and thermodynamic parameters are investigated, discussed, and compared with those of other reported materials.

2. Materials and Methods

2.1. Materials. Pyrrole (Py, >98%), ammonium persulfate (APS, 98%), potassium hydroxide (KOH, 85%), sodium nitrate ($NaNO_3$, 99%), and sodium hydroxide (NaOH, 98%) were purchased from Alfa Aesar, Karlsruhe, Germany. Hydrochloric acid (HCl, ~36%) and ethanol (EtOH, 99.5%) were obtained from Fisher Chemical, Loughborough, UK. CV (>90%) was provided by BDH Chemicals Ltd., Poole, England, UK, which was dried at 80°C for 2 h before use. All materials were used as received unless otherwise stated.

2.2. Adsorbent. PACK was prepared as described in the literature [15–18]. Briefly, HCl-doped polypyrrole (PPy) was prepared using an equimolar quantity (0.08 mol) of the monomer (Py) and the initiator (APS) in cold HCl (1 L, 0.1 M). The obtained material was washed and dried and then calcined under nitrogen at 650°C attained at 3°C/min for 2 h with four times the mass of KOH, the chemical activator, using a Carbolite MTF 12/38/250 tube furnace (Wolf Laboratories, UK). The PACK obtained was sequentially washed with 0.5 M HCl and then water until neutrality and dried.

The pH at which the surface net charges of PACK are zero (pH_{PZC}) was determined by a pH drift method described elsewhere [19, 20]. Typically, a solution of 0.1 M $NaNO_3$ was prepared from which batches of 15 mL were adjusted in the pH range 2–11 using 0.1 M HCl or 0.1 M NaOH solution and denoted as pH_i. To each sample, 0.015 g PACK was added, and the suspension was shaken intermittently for

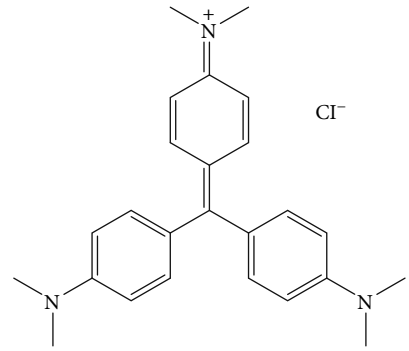

Figure 1: Chemical structure of CV.

24 h at room temperature (25 ± 1°C). Then, the samples were filtered, and the final pH (pH_f) of the solutions was measured. The pH of each sample was determined by an Orion 3 Star pH meter (Thermo Scientific, Beverly, MA, USA). pH_{PZC} was determined by plotting pH_i vs. pH_f. Experiments were performed in duplicate and in parallel with unloaded samples as references. Moreover, a zeta potential of a sample of 1 mg/mL PACK-water dispersion (without pH adjustment) was measured by dynamic light scattering (DLS) (Zetasizer Nano; Malvern Instruments Ltd., London, UK) at room temperature.

2.3. Adsorbate. The chemical structure of the adsorbate CV is shown in Figure 1. It is a well-known cationic dye with a color index number of C.I. 42555, a λ_{max} of 590 nm, a molar mass of 407.98 g/mol, and solubility in water of 16 g/L at 25°C. A stock solution (1000 ppm) of CV was prepared in deionized water and further diluted to obtain the desired working concentrations. The extinction coefficient of CV ($\mathcal{E} = 85436\ M^{-1} \cdot cm^{-1} = 0.2094\ ppm^{-1} \cdot cm^{-1}$) was obtained from a standard curve established using CV concentrations of 0.5, 1, 2, 3, and 4 ppm ($R^2 = 0.9864$), with the dye concentrations measured photometrically using a UV-Vis spectrophotometer (U-2910, Hitachi, Tokyo, Japan) with reference to λ_{max} at room temperature (25 ± 1°C).

2.4. Adsorption Experiments. Adsorption equilibrium experiments were performed using 50 mL Eppendorf tubes at CV concentrations of 50, 100, 200, 300, and 500 ppm and temperatures of 25, 35, and 45°C, using 20 mg of the adsorbent (PACK), agitated at 150 rpm using a GFL 3017 digital shaker (GFL Gesellschaft für Labortechnik mbH, Burgwedel, Germany) for 24 h. Then, the adsorbent was filtered off, and the residual CV concentrations were measured. Kinetic experiments were conducted using 1 L Erlenmeyer flasks under the following conditions: 40 mg PACK, 500 mL CV solutions (15 and 45 ppm), 150 rpm agitation, and 25°C adsorption temperature. The residual dye concentrations were measured at 0, 5, 10, 30, 45, 60, 90, and 120 min, with at least two replicate concentration measurements being performed. All experiments were performed in duplicate without pH adjustment. However, the pH value of, e.g., 50 ppm CV solution analyzed at 25 ± 1°C was found to be 6.91 ± 0.19. Regeneration trials were carried out by using solvent mixtures of acetone and 0.25 M of NaOH or HCl. However,

a pilot experiment was performed first using single eluents of NaOH, HCl, acetic acid (AA), and acetone (Ac). The results obtained were not satisfied, with less than 24% desorption obtained when NaOH or HCl was used alone. Accordingly, elution systems of 25% acetone and 75% of 0.25 NaOH or HCl were chosen, and the reusability test was performed for three cycles of adsorption-desorption processes.

2.5. Theoretical Calculations. The equilibrium adsorption capacity (q_e, mg/g) and the removal efficiency (Re, %) of PACK were determined using Equations (1) and (2), respectively:

$$q_e = \frac{(C_0 - C_e)V}{m}, \tag{1}$$

$$\text{Re } \% = \left(\frac{C_0 - C_e}{C_0}\right)100, \tag{2}$$

where C_0 and C_e are the adsorbate concentrations (mg/L) in the liquid phase before and after adsorption, V (L) is the solution volume, and m (g) is the dry mass of the adsorbent used.

The adsorption mechanism was investigated by employing the pseudo-first-order (PFO), pseudo-second-order (PSO), and intraparticle diffusion (IPD) kinetics models proposed by Lagegren and Svenska [21], Ho and McKay [22], and Weber and Morris [23], respectively. The linear forms of these three models are given by Equations (3), (4), and (5), respectively.

$$\log (q_e - q_t) = \log (q_e) - \frac{k_1 t}{2.303}, \tag{3}$$

$$\frac{t}{q_t} = \frac{1}{k_2 q_e^2} + \frac{t}{q_e}, \tag{4}$$

$$q_t = k_{id} t^{0.5} + C, \tag{5}$$

where q_t (mg/g) is the adsorption capacity at time t (min); k_1 (min^{-1}), k_2 (g/(mg·min)), and k_{id} (mg/(g·$\text{min}^{0.5}$)) are the rate constants of the PFO, PSO, and IPD models, respectively; and C (mg/g) is the y-intercept of the IPD model, giving information about the boundary layer thickness, where higher values of C indicate greater boundary layer effects [23, 24]. The initial rate (h) (mg/(g·min)) of the adsorption process is typically given by the reciprocal value of the PSO plot intercept:

$$h = k_2 q_e^2. \tag{6}$$

The adsorption isotherm was modeled with the Langmuir [25, 26], Freundlich [27], Temkin [28], and Dubinin-Radushkevich (D-R) [29] linear form models, as given in Equations (7), (8), (9), and (10), respectively.

$$\frac{C_e}{q_e} = \frac{C_e}{q_m} + \frac{1}{K_L q_m}, \tag{7}$$

$$\ln q_e = \ln K_F + \frac{1}{n} \ln C_e, \tag{8}$$

$$q_e = \frac{RT}{K_T} \ln A + \frac{RT}{K_T} \ln C_e = B \ln A + B \ln C_e, \tag{9}$$

$$\ln q_e = \ln q_m - K_{D\text{-}R} \mathcal{E}^2, \tag{10}$$

where q_m (mg/g) is the maximum monolayer capacity; K_L (L/mg), K_F (mg/g)(L/mg)$^{1/n}$, K_T (J/mol), and $K_{D\text{-}R}$ (mol^2/kJ^2) are, respectively, the Langmuir, Freundlich, Temkin, and D-R isotherm constants; T (K) is the absolute temperature, R (8.314 J/mol·K) is the universal gas constant, and A (L/mg) is the Temkin isotherm equilibrium binding constant. Basically, the Langmuir isotherm (Equation (7)) assumes monolayer adsorbent surface coverage. This can be better understood in terms of the so-called separation factor (R_L, dimensionless) given in Equation (11), which describes the isotherm shape and indicates whether the adsorption is favorable or not, as per the following criteria: $R_L > 1$, unfavorable adsorption; $R_L = 1$, linear; $0 < R_L < 1$, favorable; and $R_L = 0$, irreversible.

$$R_L = \frac{1}{1 + K_L C_0}. \tag{11}$$

Conversely, the Freundlich isotherm, Equation (8), assumes multilayer adsorption and a heterogeneous adsorbent surface. The $1/n$ value indicates the relative distribution of energy and the heterogeneity of the adsorbent sites. Thus, $1/n > 1$ represents multilayer adsorption, $1/n = 1$ denotes a linear adsorption and concentration-independent adsorption with indistinguishable energy of all sites, $1/n < 0$ indicates Langmuir-shaped adsorption, and $0.1 < 1/n < 1.0$ represents favorable adsorption conditions where heterogeneity increases as the value approaches zero [30, 31]. The Temkin isotherm, Equation (9), assumes that, at moderate concentration, the intermolecular interactions cause the heats of adsorption of all the molecules to decrease linearly with coverage. K_T is the Temkin equilibrium constant related to the maximum binding energy [32]. The D-R isotherm equation (Equation (10)) is an analog of the Langmuir equation. However, it is more general and ordinarily describes the adsorption mechanism assuming a Gaussian energy distribution onto a heterogeneous surface [33–35]. Therefore, it is only suitable for intermediate concentrations. The D-R constant, $K_{D\text{-}R}$, is the activity coefficient related to the mean sorption energy, while $\mathcal{E}$ (Equation (12)) is the Polanyi potential. The mean adsorption energy, E (kJ/mol), can be calculated using Equation (13). It provides information about the adsorbate free energy required for the transfer of one mole from infinite distance to the adsorbent surface, indicating whether the adsorption mechanism is a chemical ion exchange (9–16 kJ/mol) or physical (less than 8 kJ/mol) [28, 36, 37].

$$\mathcal{E} = RT \ln \left(1 + \frac{1}{C_e}\right), \tag{12}$$

Table 1: Properties of PACK.

Chemical composition (wt%)						BET		Adsorption capacity (mg/g)		
C	H	N	O	K	Cl	SA (m^2/g)	APD (nm)	CO_2	Pb^{2+}	MO
73.17	0.86	4.70	20.37	0.40	0.50	2871	2.3	50	50	521

BET: Brunauer–Emmett–Teller; SA: surface area; APD: average pore diameter; MO: methyl orange.

$$E = \frac{1}{(2K_{\text{D-R}})^{0.5}}. \quad (13)$$

The effect of heat on the adsorption system was determined using the thermodynamic parameters Gibbs free energy change (ΔG°), enthalpy change (ΔH°), and entropy change (ΔS°), which are expressed by the Van't Hoff equation [38]:

$$\ln K_0 = \frac{\Delta S^\circ}{R} - \frac{\Delta H^\circ}{RT} = -\frac{\Delta G^\circ}{RT}, \quad (14)$$

$$K_0 = \frac{q_e}{C_e}, \quad (15)$$

where K_0 (L/g) is the apparent equilibrium constant.

3. Results and Discussion

3.1. Characterization. The essential features of the adsorbent PACK, including its structural and surface properties as well as its efficacies as an adsorbent of gasses, heavy metal ions, and anionic dyes represented by carbon dioxide (CO_2), lead ions (Pb^{2+}), and methyl orange (MO), respectively, have been reported by Alghamdi et al. [15–17] and Sevilla et al. [18] (Table 1). Furthermore, to obtain insight into the surface charge, the pH at which the net surface charge is zero (pH_{PZC}) was estimated and found to be 6.35 (Figure 2). Thus, the surface is positively charged below pH 6.35 and negatively charged above pH 6.35. Moreover, the zeta potential at neutral pH (-30.6 mV, see Figure S1) indicated a negative surface which further supports the pH_{PZC} result.

3.2. Effect of Contact Time and Kinetic Studies. Figure 3 shows the time profile of CV adsorption onto PACK for two different initial concentrations (15 and 45 ppm). Figure 4 shows a histogram representing the values of the adsorption efficiency (Re, %) as well as the capacities at the first adsorption phase (q_{5t}, 5 min) and at equilibrium (q_e, 60 min). Clearly, the adsorption is initially fast (~5 min), indicating an abundance of readily available active sites on the adsorbent surface. Thereafter, the adsorption rate slows dramatically as the active sites are gradually saturated by the adsorbate molecules, reaching equilibrium after ~60 min. Moreover, the data indicate that more than 80% of the adsorbent sites are occupied in the first 5 min (Figure 3). It is also observed that as the initial dye concentration increases, the adsorption capacity (q_e) increases while the efficiency (Re) decreases. The initial rapid adsorption (i.e., in the first 5 min) indicates a chemisorption process. However, for the second phase, the profile suggests a physisorption mechanism, which is possibly governed by a diffusion mechanism [39].

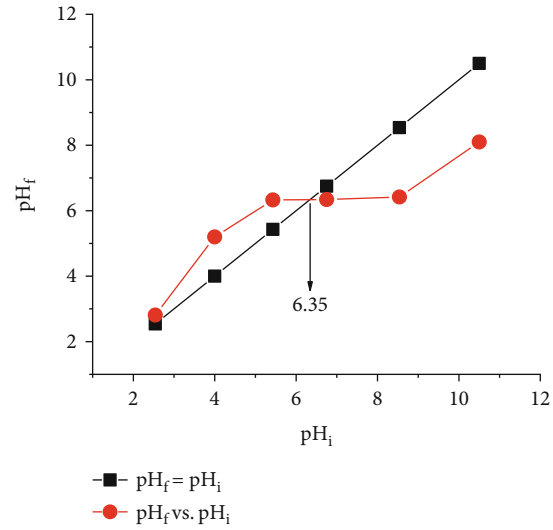

Figure 2: Point of zero charge for PACK adsorbent.

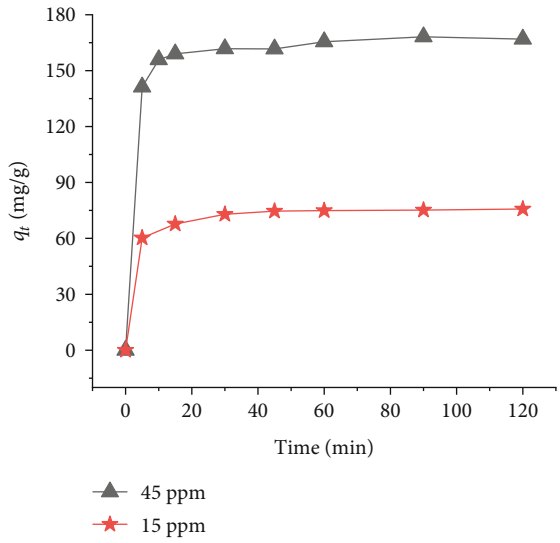

Figure 3: Effect of contact time on the adsorption of CV onto PACK.

The mechanism involved in this adsorption system was investigated using PFO, PSO, and IPD kinetic models (Figures 5, 6, and 7), as described by Equations (3), (4), and (5), respectively. The corresponding kinetic parameters and correlation coefficients are presented in Table 2. As can be seen, the relatively higher value of the correlation coefficient, which is an important criterion in the determination of good fit, for the PSO model ($R^2 \geq 0.9996$) compared to those of the PFO ($R^2 \leq 0.8392$) and IPD ($R^2 \leq 0.8143$) models as well as

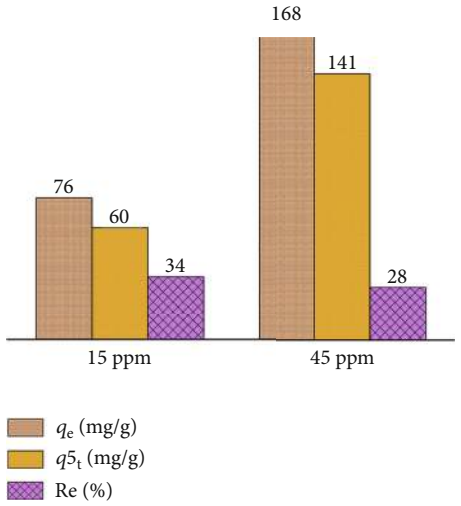

Figure 4: Graphical illustration of the adsorption of CV (C_0 = 15 and 45 ppm) on PACK after 5 min (q_{5t}, the initial adsorption phase) and at equilibrium (q_e), along with efficiency (%) values. Conditions: adsorbate volume = 500 mL; temperature = 25°C; adsorbent mass = 0.04 g; agitation = 150 rpm; apparent equilibrium time = 90 min.

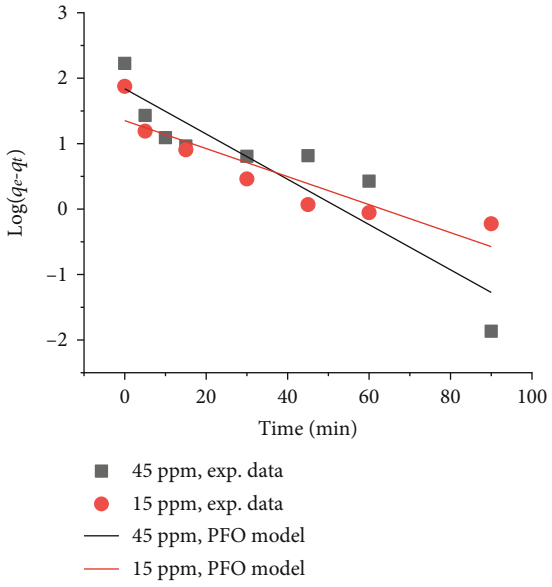

Figure 5: PFO kinetic plot for the adsorption of CV onto PACK. Conditions: C_0 = 15, 45 ppm; adsorbate volume = 500 mL; temperature = 25°C; adsorbent = 0.04 g; agitation = 150 rpm; time = 90 min.

the very close similarity of the experimental and PSO model adsorption capacity (q_e) values indicates that the adsorption mechanism is best described by the PSO model. The poor fit of the IPD ($R^2 \leq 0.8143$) model reveals the negligible effect of intraparticle diffusion on the rate-controlling step. Moreover, the intercept deviation from the origin indicates the involvement of a film-diffusion mechanism. The high value of the intercept C, which is the measure of the film boundary

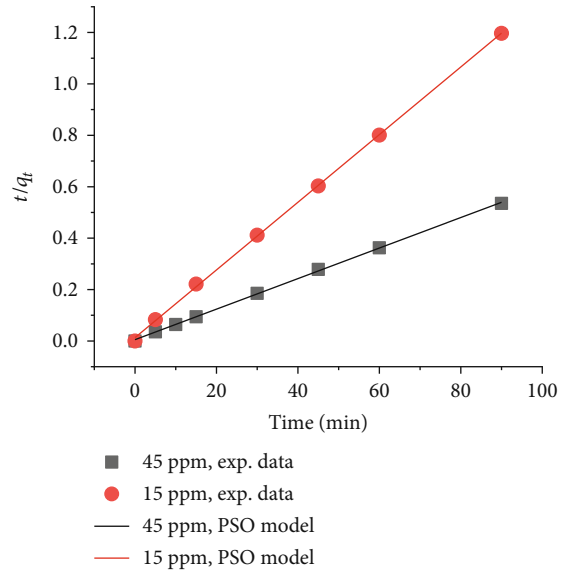

Figure 6: PSO kinetic plot for the adsorption of CV onto PACK.

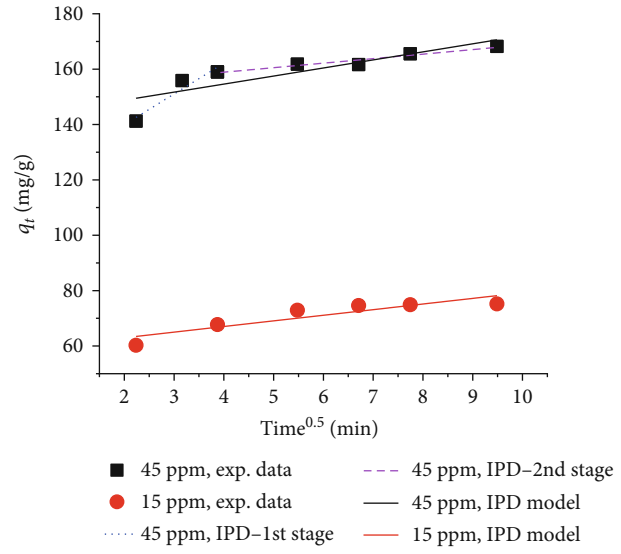

Figure 7: Webber-Morris intraparticle diffusion plot for the adsorption of CV onto PACK (see Figure 4 for conditions).

thickness, reflects the significant effect of external film resistance on the adsorption mechanism. Moreover, the IPD plot indicates the presence of more than one single mechanism. Generally, the fast adsorption rate in the first few minutes is not recognized as a rate-limiting step and can be explained by the abundance of CV dye molecules and PACK active sites in the adsorption system. However, the two-stage IPD plot for the adsorption process at a CV concentration of 45 ppm (Figure 7) may indicate a gradual adsorption controlled by a boundary layer (stage 1) followed by a slow adsorption controlled by intraparticle diffusion and equilibrium processes (stage 2); data of the two-stage IPD model are given in the supporting information, Table S1.

Table 2: Kinetic parameters for the adsorption of CV onto PACK.

C_0 (mg/L)	q_e-exp (mg/g)	PFO			PSO			IPD			
		q_e (mg/g)	k_1 (1/min)	R^2	q_e (mg/g)	k_2 (g/(mg·min))	R^2	h (mg/(g·min))	k_{id} (mg/(g·min$^{0.5}$))	C (mg/g)	R^2
15	75.77	22.53	0.049	0.8291	75.99	0.013	0.9997	76.45	2.031	58.92	0.8143
45	168.19	69.07	0.080	0.8392	168.35	0.0069	0.9996	145.39	2.910	142.96	0.7450

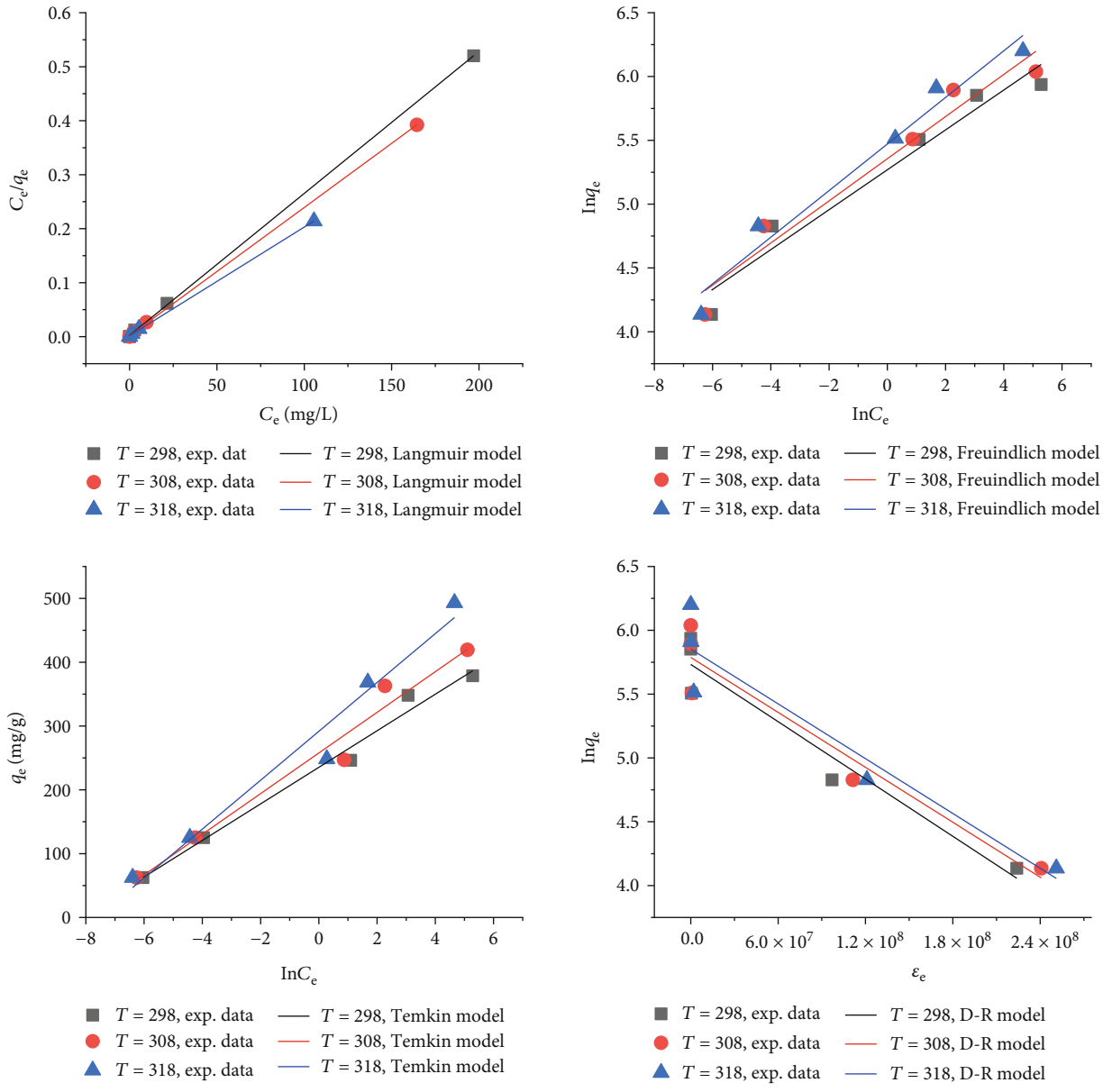

Figure 8: Langmuir, Freundlich, Temkin, and D-R isotherm plots for CV adsorption onto PACK.

3.3. Adsorption Isotherms. Adsorption isotherms generally describe the way in which an adsorbate interacts with an adsorbent when equilibrium is attained at a certain temperature. In this study, the adsorption system was evaluated at 25, 35, and 45°C, and the experimental data were fitted into four models expressed by Equations (7)–(10) (Figure 8), and the calculated parameters are presented in Table 3. The goodness of fit for the experimental data was found to be in the order Langmuir ($R^2 \geq 0.9997$) > Temkin ($R^2 \leq 0.9853$) > Freundlich ($R^2 \leq 0.9688$) > D-R ($R^2 \leq 0.9382$). The maximum adsorption capacity (the monolayer surface coverage) (q_m, mg/g), for the initial CV concentration range 50–500 ppm, was increased from 380.2 to 497.5 mg/g as the temperature increases from 298 to 318 K. Over the same

Table 3: Langmuir, Freundlich, Temkin, and D-R isotherm parameters for CV adsorption onto PACK.

(a)

Temp. (K)	Langmuir				Freundlich			
	q_m (mg/g)	K_L (L/mg)	R_L (C_0 (mg/L) = 50 – 500)	R^2	K_F (mg/g) (L/mg)$^{1/n}$	$1/n$	n	R^2
298	380.23	1.13	0.0172–0.0018	0.9999	194.23	0.156	6.41	0.9535
308	421.94	1.23	0.0159–0.0016	0.9999	211.85	0.165	6.06	0.9534
318	497.51	1.26	0.0157–0.0016	0.9997	237.75	0.183	5.48	0.9688

(b)

T (K)	Temkin				Dubinin-Radushkevich (D-R)			
	A (L/mg)	K_T (J/mol)	B	R^2	$K_{D\text{-}R}$ (mol^2/J^2)	q_m (mg/g)	E (kJ/mol)	R^2
298	3693.96	86.50	28.643	0.9853	7.48×10^{-9}	308.93	8.174	0.9382
308	3271.63	80.40	31.851	0.9719	7.18×10^{-9}	326.24	8.345	0.9285
318	2031.85	69.04	38.294	0.9690	7.16×10^{-9}	348.39	8.357	0.9071

Table 4: Thermodynamic parameters for the adsorption of CV onto PACK.

C_0 (mg/L)	T (K)	ln K_0	ΔG° (kJ/mol)	ΔH° (kJ/mol)	ΔS° (J/mol·K)	R^2
	298	10.1725	−5.7472			
50	308	10.3957	−5.9956	14.0845	131.942	0.9844
	318	10.5292	−6.2240			
	298	8.7861	−5.3842			
100	308	9.0738	−5.6474	18.5563	135.438	0.9880
	318	9.2561	−5.8833			
	298	4.4129	−3.6780			
200	308	4.6391	−3.8015	32.5018	145.214	0.9260
	318	5.2423	−4.3802			
	298	2.7850	−2.5376			
300	308	3.6251	−3.2979	56.9083	214.378	0.9942
	318	4.2276	−3.8115			
	298	0.6537	1.0532			
500	308	0.9357	0.1702	34.8243	121.823	0.9496
	318	1.5416	−1.1443			

temperature range, the values of the heterogeneity factor $1/n$ (0.156–0.183) and separation factor (R_L) (0.016–0.002) indicate favorable adsorption. The decrease in the values of the Temkin equilibrium binding constant (A) with temperature increase indicates favorable adsorption process at high temperatures. According to the D-R model, the values of the mean adsorption energy, E (kJ/mol), over the tested temperatures are in the range 8.174–8.357 kJ/mol, indicating a predominantly physisorption process (i.e., E (chemical) > 9; E (physical) < 8) [28, 36]. As the values of the E are in the boundary between the two mechanisms, the involvement of the ion exchange adsorption mechanism cannot be ruled out. Such electrostatic interaction is expected between the positively charged CV particles and negative sites on PACK.

3.4. Adsorption Thermodynamics. The values of Gibbs free energy (ΔG°), enthalpy (ΔH°), and entropy (ΔS°) changes obtained for CV concentrations of 50, 100, 200, 300, and 500 ppm are given in Table 4. The negative values of ΔG° indicate the spontaneity and feasibility of the adsorption, whereas the positive values of ΔH° and ΔS° indicate the endothermic nature and increase in randomness of the process, respectively [40]. According to the data obtained under the applied conditions, the adsorption process is more favored at low concentrations and at high temperatures (Table 4). It is known that the value of ΔG° for chemisorption (−80 to −400 kJ/mol) is higher than that of physical adsorption (from 0 to −20 kJ/mol). Moreover, a value of ΔH° less than 40 kJ/mol suggests a physical process [41]. Here, the ranges of ΔG° and ΔH° values indicate a physical adsorption mechanism, supporting our earlier conclusion.

Figure 9 is a schematic presentation for the adsorption mechanism in which π-π and ionic interactions are dominant. This is in line with the results predicted by the adsorption models discussed above. Thus, the physisorption mechanism is practically superior; however, chemical

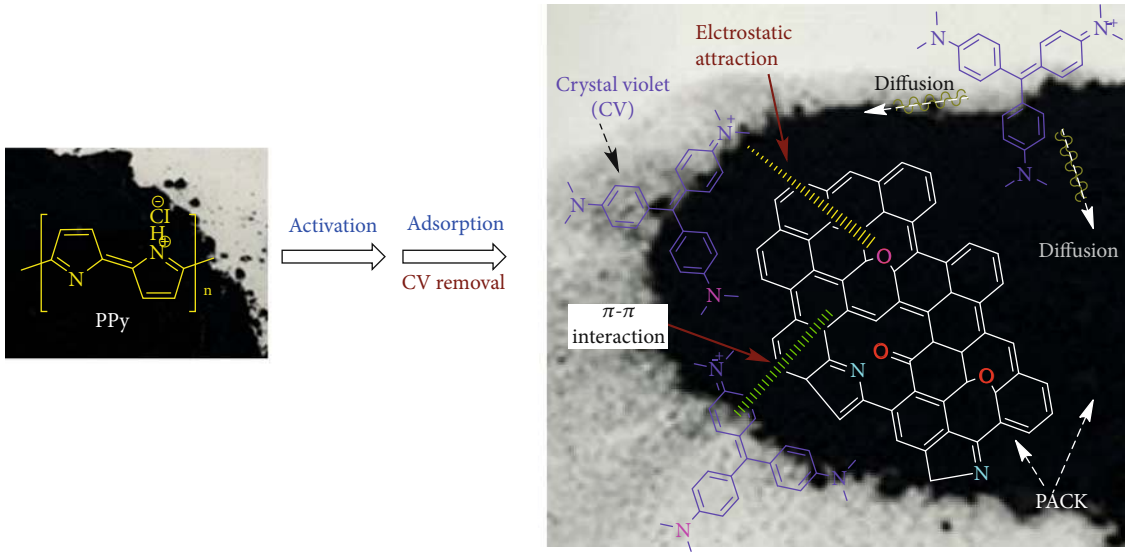

Figure 9: Schematic presentation of the adsorption mechanism of the cationic dye crystal violet by PACK adsorbent.

interaction involving strong ionic bonds and ion exchange cannot be ignored, a case that is evinced by the results of isotherms and thermodynamic parameter values, which are generally in the region of the physical process but closer to chemical limits. Moreover, the effect of the diffusion process in the adsorption mechanism is also expected at least in the last stage of adsorption.

3.5. Reusability. As the reusability of the adsorbent is of crucial importance in the economic development, efficient protocols for adsorbate recovery and adsorbent regeneration have to be established; however, common adsorbents vary greatly in their stability and applicability to be regenerated. Figure 10 illustrates the chemical regeneration efficiency calculated according to [5]

$$\text{Desorption}\,(\%) = \left(\frac{\text{Desorbed mass}}{\text{Adsorbed mass}}\right)100. \qquad (16)$$

The low desorption efficiency of a single solvent elution system (NaOH, HCl) may be due to ion competition, indicating high comparative affinity of CV dye toward PACK (Figure 10; only cycle 1 is presented). However, NaOH shows better desorption performance of CV than HCl, possibly due to electrostatic repulsion at pH above pH_{PZC} [5].

When acetone was added to the above single solvents, the regeneration efficiency was enhanced. As shown in Figure 10, the desorption efficiency reduced about 4 and 11% when the binary eluents NaOH/Ac and HCl/Ac were used, respectively. The results generally indicate a total mass recovery of CV of about 72% after three cycles of the adsorption-desorption process. The reduced efficiency (28%) could be due to incomplete desorption of CV [42]. The results indicate the reusability of the adsorbent with possible regeneration enhancement; however, it necessitates further optimization of the regeneration conditions including solvents types, concentrations, solution pH, etc.

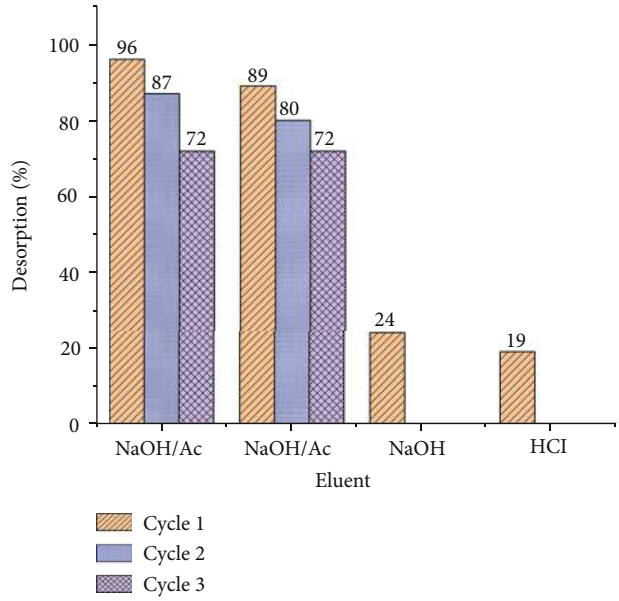

Figure 10: Desorption percentage of CV from PACK after three cycles using solvent mixtures (NaOH/acetone or HCl/acetone) or single solvent (NaOH or HCl; only cycle one presented).

3.6. Relative Performance of PACK. For comparative purposes, the values of adsorption capacity, q_m (mg/g), of several adsorbents reported in the literature are provided in Table 5. Furthermore, information on the adsorbent source, reusability, and adsorption conditions has also been tabulated. As can be seen, the q_m of PACK for CV is 497.51 mg/g, which is well positioned with respect to the listed materials. The differences in the adsorption capacities are due to the variety in the chemical and morphological properties of the adsorbents, including their functional groups, surface areas, and porosities. However, the suitability of a potential adsorbent is generally assessed in terms of efficiency, availability, reusability, and cost-effectiveness. The naturally available and the

Table 5: Comparison of the CV adsorption capacities of various reported adsorbents.

Adsorbent	q_m (mg/L)	Adsorption conditions				Ref.	Source type
		C_o (mg/L)	pH	T (°C)	Adsorbent dosage (g/L)		
NaOH-modified rice husk (NMRH)	44.88	50	8	20	1.0	[44]	Agriculture
Granulated-activated carbon	90.91	5-15	11	40	1.0	[5]	Commercial
Natural zeolite	177.75	20-200	10	25	2.0	[45]	Natural clay
Merck-activated carbon	84.11	30-80	7	25	1.0	[45]	Commercial
$ZnCl_2$-activated carbon (ZCAC)	142.85	20-90	8	25	1.0	[19]	Agriculture
Jute fiber carbon	27.99	20-110	8	30	1.0	[46]	Agriculture
Phosphoric acid-activated carbon (PAAC)	60.38	10-40	6	RT	3.0	[10]	Agriculture
Sulfuric acid-activated carbon (SAAC)	85.68	10-40	6	RT	2.0	[10]	Agriculture
F. orientalis L.-activated carbon	769.23	200-800	—	25	0.8	[47]	Agriculture
Biochar from palm kernel shell (BC-PKS)	24.45	50-500	7	25	16.7	[48]	Biomass
Palm kernel fiber	78.9	20-180	7.2	25	2.0	[49]	Agriculture
Tomato waste nanoporous carbon (TWNC)	64.52	20-350	8	40	2.0	[50]	Biomass
PACK	497.51	50-500	6.9	45	0.8	This work	Synthetic

agricultural and industrial wastes may be inexpensive adsorbents, but they are less efficient. In many cases, modification of such materials has increased their adsorption efficiencies. Conversely, the synthetic adsorbents, including activated carbon, exhibit better performances in the removal of water pollutants ([16, 43]). However, the source of the carbonaceous materials, processing, and activation conditions are important factors in the final properties of the carbon. The excellent adsorptive performance of PACK can be ascribed to the properties discussed above.

4. Conclusions

Here, the adsorption efficiency of PACK for the removal of CV from aqueous solutions was investigated. Batch adsorption processes were performed to investigate the effects of contact time (0–120 min, and up to 24 h), initial CV concentration (50–500 mg/L), and temperature (25–45°C). The adsorption kinetics, evaluated using PFO, PSO, and IPD models, revealed that the PSO model provided a better fit ($R^2 \geq 0.9996$). Also, the result indicates an adsorption rate-limiting step dominantly controlled by film diffusion. The equilibrium data, fitted to Langmuir, Freundlich, Temkin, and D-R isotherms, were found to be best expressed by the Langmuir model with a maximum monolayer capacity, q_m, of 497.51 mg/g. The thermodynamic studies indicated a spontaneous and endothermic adsorption system in which the spontaneity slightly increases with temperature and decreases with initial CV concentration. The values of ΔG° and ΔH° are clearly positioned in the range indicating a physisorption mechanism, i.e., $0 > \Delta G^\circ \geq -20$ kJ/mol and $\Delta H^\circ < 40$ kJ/mol. Overall, these results show that the PACK is a promising adsorbent for the removal of CV and potentially other cationic dyes, from industrial effluent.

Data Availability

Data that support the findings of this study are included within the article and supplementary information file.

Conflicts of Interest

The authors declared no potential conflicts of interest with respect to the research, authorship, and/or publication of this article.

Acknowledgments

The authors extend their appreciation to the Deanship of Scientific Research at King Saud University for funding this work through Research Group No. RGP-1438-040.

Supplementary Materials

The following are available. Figure S1: zeta potential results of PACK adsorbent in water. Table S1: parameters of the two-stage intraparticle diffusion (IPD) model. *(Supplementary Materials)*

References

[1] H. Hayzoun, A. Ouammou, O. Saidi, F. Khalil, and L. Bouayyadi, "Evaluation de la qualité bactériologique et chimique du Sebou, Maroc (assessment of the bacteriological and chemical quality of the Sebou River, Morocco)," *Journal of Materials and Environmental Science*, vol. 5, no. S2, pp. 2438–2443, 2014.

[2] S. Komissarchik and G. Nyanikova, "Test systems and a method for express detection of synthetic food dyes in drinks," *LWT-Food Science and Technology*, vol. 58, no. 2, pp. 315–320, 2014.

[3] J.-H. Huang, K.-L. Huang, S.-Q. Liu, A. T. Wang, and C. Yan, "Adsorption of rhodamine B and methyl orange on a hypercrosslinked polymeric adsorbent in aqueous solution," *Colloids and Surfaces A: Physicochemical and Engineering Aspects*, vol. 330, no. 1, pp. 55–61, 2008.

[4] A. Azarkohan, F. Shemirani, and M. Alvand, "Fast analysis of water samples for trace amount of crystal violet dye based on solid phase extraction using nanoporous SBA-3 prior to determination by fiber optic-linear array detection

spectrophotometry," *Journal of Chemistry*, vol. 2013, Article ID 530843, 8 pages, 2013.

[5] M. Abbas, Z. Harrache, and M. Trari, "Removal of gentian violet in aqueous solution by activated carbon equilibrium, kinetics, and thermodynamic study," *Adsorption Science & Technology*, vol. 37, no. 7-8, pp. 566–589, 2019.

[6] A. Adak, M. Bandyopadhyay, and A. Pal, "Removal of crystal violet dye from wastewater by surfactant-modified alumina," *Separation and Purification Technology*, vol. 44, no. 2, pp. 139–144, 2005.

[7] L. Ayed, K. Chaieb, A. Cheref, and A. Bakhrouf, "Biodegradation of triphenylmethane dye malachite green by *Sphingomonas paucimobilis*," *World Journal of Microbiology and Biotechnology*, vol. 25, no. 4, pp. 705–711, 2009.

[8] Y. Benjelloun, A. Lahrichi, S. Boumchita et al., "Removal of crystal violet by wet oxidation with H_2O_2 over an iron oxide catalyst synthesized from fly ash," *Journal of Materials and Environmental Sciences*, vol. 8, no. 7, pp. 2259–2269, 2017.

[9] A. Mittal, J. Mittal, A. Malviya, D. Kaur, and V. K. Gupta, "Adsorption of hazardous dye crystal violet from wastewater by waste materials," *Journal of Colloid and Interface Science*, vol. 343, no. 2, pp. 463–473, 2010.

[10] S. Senthilkumaar, P. Kalaamani, and C. Subburaam, "Liquid phase adsorption of crystal violet onto activated carbons derived from male flowers of coconut tree," *Journal of Hazardous Materials*, vol. 136, no. 3, pp. 800–808, 2006.

[11] K. Akansha, D. Chakraborty, and S. G. Sachan, "Decolorization and degradation of methyl orange by *Bacillus stratosphericus* SCA1007," *Biocatalysis and Agricultural Biotechnology*, vol. 18, article 101044, 2019.

[12] S. Ledakowicz, M. Solecka, and R. Zylla, "Biodegradation, decolourisation and detoxification of textile wastewater enhanced by advanced oxidation processes," *Journal of Biotechnology*, vol. 89, no. 2-3, pp. 175–184, 2001.

[13] I. A. Salem, "Activation of H_2O_2 by amberlyst-15 resin supported with copper(II)-complexes towards oxidation of crystal violet," *Chemosphere*, vol. 44, no. 5, pp. 1109–1119, 2001.

[14] L. Zhao, W. Zou, L. Zou, X. He, J. Song, and R. Han, "Adsorption of methylene blue and methyl orange from aqueous solution by iron oxide-coated zeolite in fi xed bed column: predicted curves," *Desalination and Water Treatment*, vol. 22, no. 1-3, pp. 258–264, 2012.

[15] A. A. Alghamdi, A. B. al-Odayni, W. S. Saeed, A. al-Kahtani, F. A. Alharthi, and T. Aouak, "Efficient adsorption of lead (II) from aqueous phase solutions using polypyrrole-based activated carbon," *Materials*, vol. 12, no. 12, 2019.

[16] A. A. Alghamdi, A. B. al-Odayni, W. S. Saeed et al., "Adsorption of azo dye methyl orange from aqueous solutions using alkali-activated polypyrrole-based graphene oxide," *Molecules*, vol. 24, no. 20, p. 3685, 2019.

[17] A. A. Alghamdi, A. F. Alshahrani, N. H. Khdary, F. Alharthi, H. Alattas, and S. Adil, "Enhanced CO_2 adsorption by nitrogen-doped graphene oxide sheets (N-GOs) prepared by employing polymeric precursors," *Materials*, vol. 11, no. 4, p. 578, 2018.

[18] M. Sevilla, P. Valle-Vigón, and A. B. Fuertes, "N-doped polypyrrole-based porous carbons for CO_2 capture," *Advanced Functional Materials*, vol. 21, no. 14, pp. 2781–2787, 2011.

[19] K. Doke, M. Yusufi, R. Joseph, and E. M. Khan, "Comparative adsorption of crystal violet and Congo red onto ZnCl2Activated carbon," *Journal of Dispersion Science and Technology*, vol. 37, no. 11, pp. 1671–1681, 2015.

[20] S. Lazarević, I. Janković-Častvan, D. Jovanović, S. Milonjić, D. Janaćković, and R. Petrović, "Adsorption of Pb^{2+}, Cd^{2+} and Sr^{2+} ions onto natural and acid-activated sepiolites," *Applied Clay Science*, vol. 37, no. 1-2, pp. 47–57, 2007.

[21] S. Lagegren and B. Svenska, "Zur theorie der sogenannten adsorption geloester stoffe," *Vaternskapsakad Handlingar*, vol. 24, no. 4, pp. 1–39, 1898.

[22] Y.-S. Ho and G. McKay, "Pseudo-second order model for sorption processes," *Process Biochemistry*, vol. 34, no. 5, pp. 451–465, 1999.

[23] W. J. Weber and J. C. Morris, "Kinetics of adsorption on carbon from solution," *Journal of the Sanitary Engineering Division*, vol. 89, no. 2, pp. 31–59, 1963.

[24] S. Allen, G. McKay, and K. Khader, "Intraparticle diffusion of a basic dye during adsorption onto sphagnum peat," *Environmental Pollution*, vol. 56, no. 1, pp. 39–50, 1989.

[25] I. Langmuir, "The adsorption of gases on plane surfaces of glass, mica and platinum," *Journal of the American Chemical Society*, vol. 40, no. 9, pp. 1361–1403, 1918.

[26] I. W. Mwangi, J. C. Ngila, and J. O. Okonkwo, "A comparative study of modified and unmodified maize tassels for removal of selected trace metals in contaminated water," *Toxicological & Environmental Chemistry*, vol. 94, no. 1, pp. 20–39, 2012.

[27] H. Freundlich and W. Heller, "The adsorption of cis- and trans-azobenzene," *Journal of the American Chemical Society*, vol. 61, no. 8, pp. 2228–2230, 1939.

[28] S. Banerjee and M. Chattopadhyaya, "Adsorption characteristics for the removal of a toxic dye, tartrazine from aqueous solutions by a low cost agricultural by-product," *Arabian Journal of Chemistry*, vol. 10, pp. S1629–S1638, 2017.

[29] M. Dubinin, "The equation of the characteristic curve of activated charcoal," *Doklady Akademii Nauk SSSR*, vol. 55, pp. 327–329, 1947.

[30] R. Gong, J. Ye, W. Dai et al., "Adsorptive removal of methyl orange and methylene blue from aqueous solution with finger-citron-residue-based activated carbon," *Industrial & Engineering Chemistry Research*, vol. 52, no. 39, pp. 14297–14303, 2013.

[31] S. Liu, "Cooperative adsorption on solid surfaces," *Journal of Colloid and Interface Science*, vol. 450, pp. 224–238, 2015.

[32] K. K. Choy, G. McKay, and J. F. Porter, "Sorption of acid dyes from effluents using activated carbon," *Resources, Conservation and Recycling*, vol. 27, no. 1-2, pp. 57–71, 1999.

[33] N. Ayawei, A. N. Ebelegi, and D. Wankasi, "Modelling and interpretation of adsorption isotherms," *Journal of Chemistry*, vol. 2017, Article ID 3039817, 11 pages, 2017.

[34] O. Çelebi, Ç. Üzüm, T. Shahwan, and H. N. Erten, "A radiotracer study of the adsorption behavior of aqueous Ba^{2+} ions on nanoparticles of zero-valent iron," *Journal of Hazardous Materials*, vol. 148, no. 3, pp. 761–767, 2007.

[35] C. Travis and E. L. Etnier, "A survey of sorption relationships for reactive solutes in soil," *Journal of Environmental Quality*, vol. 10, no. 1, pp. 8–17, 1981.

[36] R. Donat, A. Akdogan, E. Erdem, and H. Cetisli, "Thermodynamics of Pb^{2+} and Ni^{2+} adsorption onto natural bentonite from aqueous solutions," *Journal of Colloid and Interface Science*, vol. 286, no. 1, pp. 43–52, 2005.

[37] M. Saeed, "Adsorption profile and thermodynamic parameters of the preconcentration of Eu (III) on 2-thenoyltrifluoroacetone loaded polyurethane (PUR) foam," *Journal of Radioanalytical and Nuclear Chemistry*, vol. 256, no. 1, article 5116460, pp. 73–80, 2003.

[38] A. M. Aljeboree, A. N. Alshirifi, and A. F. Alkaim, "Kinetics and equilibrium study for the adsorption of textile dyes on coconut shell activated carbon," *Arabian Journal of Chemistry*, vol. 10, pp. S3381–S3393, 2017.

[39] J. Ma, F. Yu, L. Zhou et al., "Enhanced adsorptive removal of methyl orange and methylene blue from aqueous solution by alkali-activated multiwalled carbon nanotubes," *ACS Applied Materials & Interfaces*, vol. 4, no. 11, pp. 5749–5760, 2012.

[40] R. Elmoubarki, F. Mahjoubi, H. Tounsadi et al., "Adsorption of textile dyes on raw and decanted Moroccan clays: kinetics, equilibrium and thermodynamics," *Water resources and industry*, vol. 9, pp. 16–29, 2015.

[41] F. Krika and O. F. Benlahbib, "Removal of methyl orange from aqueous solution via adsorption on cork as a natural and low-coast adsorbent: equilibrium, kinetic and thermodynamic study of removal process," *Desalination and Water Treatment*, vol. 53, no. 13, pp. 3711–3723, 2013.

[42] M. Hayasi and M. Karimi, "Synthesis of poly (styrene-co-methacrylic acid)-coated magnetite nanoparticles as effective adsorbents for the removal of crystal violet and rhodamine B: a comparative study," *Polymer Bulletin*, vol. 74, no. 6, pp. 1995–2016, 2017.

[43] D. Chen, J. Chen, X. Luan, H. Ji, and Z. Xia, "Characterization of anion-cationic surfactants modified montmorillonite and its application for the removal of methyl orange," *Chemical Engineering Journal*, vol. 171, no. 3, pp. 1150–1158, 2011.

[44] S. Chakraborty, S. Chowdhury, and P. D. Saha, "Adsorption of crystal violet from aqueous solution onto NaOH-modified rice husk," *Carbohydrate Polymers*, vol. 86, pp. 1533–1541, 2011.

[45] M. Sarabadan, H. Bashiri, and S. M. Mousavi, "Removal of crystal violet dye by an efficient and low cost adsorbent: Modeling, kinetic, equilibrium and thermodynamic studies," *Korean Journal of Chemical Engineering*, vol. 36, pp. 1575–1586, 2019.

[46] K. Porkodi and K. V. Kumar, "Equilibrium, kinetics and mechanism modeling and simulation of basic and acid dyes sorption onto jute fiber carbon: Eosin yellow, malachite green and crystal violet single component systems," *Journal of hazardous Materials*, vol. 143, pp. 311–327, 2007.

[47] T. Aysu and M. Küçük, "Removal of crystal violet and methylene blue from aqueous solutions by activated carbon prepared from *Ferula orientalis*," *International Journal of Environmental Science and Technology*, vol. 12, pp. 2273–2284, 2015.

[48] P. P. Kyi, J. O. Quansah, C.-G. Lee, J.-K. Moon, and S.-J. Park, "The Removal of Crystal Violet from Textile Wastewater Using Palm Kernel Shell-Derived Biochar," *Applied Sciences*, vol. 10, p. 2251, 2020.

[49] G. O. El-Sayed, "Removal of methylene blue and crystal violet from aqueous solutions by palm kernel fiber," *Desalination*, vol. 272, pp. 225–232, 2011.

[50] F. Güzel, H. Sayğılı, G. A. Sayğılı, and F. Koyuncu, "Decolorisation of aqueous crystal violet solution by a new nanoporous carbon: Equilibrium and kinetic approach," *Journal of Industrial and Engineering Chemistry*, vol. 20, pp. 3375–3386, 2014.